The 7th International Supercritical CO_2 Power Cycles Symposium
February 21 – 24, 2022, San Antonio, Texas
Paper # 138

CFD Evaluation of Shroud Gap Performance Effects on a Supercritical CO2 Radial Inflow Turbine

David W. Stevens
Staff Engineer
Peregrine Turbine Technologies LLC
Wiscasset, Maine

ABSTRACT

Reliable turbomachinery requires clearance between rotating and static components to prevent collision damage caused by differential thermal growth, rotordynamics, and manufacturing tolerances. On the contrary, clearance between rotating turbine or compressor blades and adjacent static shroud components negatively impacts overall turbomachinery efficiency.

Supercritical carbon dioxide (sCO2) turbomachinery can be physically much smaller than equivalently sized gas or steam turbines due the increased density of the working fluid. Reducing the overall size of the turbomachine can be advantageous to maintenance, portability, cost, and more. Conversely, the small physical scale requires tightly controlled rotor stator clearances to maintain machine reliability and performance.

The Peregrine Turbine Technologies sCO2 turbopump utilizes a single 1.6 in (40.6 mm) diameter radial inflow turbine to provide 454hp (339kW) to two centrifugal compressors. 3D computational fluid dynamics (CFD) models with varying blade tip shroud clearances were constructed in ANSYS CFX to evaluate efficiency losses and mass flow rate changes. CFD model results are compared to existing models used for determining shroud gap losses in non-supercritical turbomachinery.

NOMENCLATURE

Symbol		Greek Symbol	
b	Blade height	ε	Shroud clearance
h	Enthalpy	η	Efficiency
k	Turbulent kinetic energy	ω	Turbulence frequency
N	Rotor speed		
p	Pressure (absolute)	Subscripts	
P	Power (shaft)	t	Total conditions
PR	Pressure ratio	s	Static conditions
Re	Reynolds number	i	Turbine blade inlet and exit
T	Temperature	1	Compressor inlet
u	x component of velocity	3	Compressor discharge
v	y component of velocity	4	Turbine inlet (nozzle inlet)
W	Mass flow	4.1	Turbine blade inlet
w	z component of velocity	4.3	Turbine blade exit
y+	Non dimensional wall distance		
Z	Blade or vane count		

INTRODUCTION

Supercritical carbon dioxide (sCO2) technology has the capability to improve the performance, footprint, and cost of fossil, nuclear, and solar energy power cycles. Turbomachinery is the heart almost all current sCO2 power cycle designs. As a turbomachinery working fluid, sCO2 features density orders of magnitude greater than air or steam. This yields extremely power dense machine designs with much smaller components. Such designs are more akin to rocket engine turbopumps than conventional gas or steam turbines currently in wide use across various applications. Additionally, sCO2 features excellent compressibility near the critical point which yields overall improved machine efficiency.

Figure 1: PTT 1MW turbopump development, HPT rotor, nozzle, and exhaust (sectioned).

While the high density and low viscosity of sCO2 allows for compact machinery and low viscous losses these properties can also be problematic at locations where leakage losses can have significant impacts on machine performance such as rotor stator tip / shroud gaps. While smaller shroud clearances reduce cross blade leakage and increase efficiency, clearances that are too small will result in collision damage caused by differential thermal growth, rotodynamic instabilities, and poor manufacturing tolerances. Determining appropriate blade tip or shroud gaps in turbomachinery has consistently been a balance between machine performance and reliability.

The Peregrine Turbine Technologies 1MW Turbopump utilizes a single radial inflow turbine to provide 454hp (339kW) to two shrouded centrifugal compressors. Turbopump specifications are detailed in Table 1. The design depicted in Figure 1 is the development high pressure (HP) turbine designed primarily for robustness and reliability during initial testing of the turbopump at the Sandia National Labs, Brayton Lab in Albuquerque, New Mexico.

Table 1: Peregrine Turbine Technologies 1MW Turbopump Specifications

	General		Turbine
N	118000 rpm	Z_{stator}	8
W	12.125 lbm/s (5.5kg/s)	Z_{rotor}	17
p_3	6280 psi (43.3 MPa)	P	454 hp (338.5 kW)
T_3	190.7 °F (361 K)	η_{tt}	90.40%
PR_{1-3}	5.5	PR_{4-5}	1.4
p_4	6135 psi (42.3 MPa)	D	1.6 in (40.6 mm)
T_4	1381.2 °F (1022.7 K)		

Initial aerodynamic design of the development HP turbine was performed using AxSTREAM® 1D mean line analysis. The design featured a total – total isentropic efficiency 90.4% with a 0.005in (0.127mm) uniform shroud gap. Reliability oriented features include thick trailing and leading edges on the turbine blades and nozzle vanes. These design features were motivated by findings by Fleming and Kruizenga [1] detailing erosion and corrosion of sCO2 turbine rotor and stator vanes. In addition to the thick blades, a turbine with a uniform 0.025in (0.635mm) shroud line cut was manufactured to further ensure machine robustness during initial testing while sacrificing efficiency. This proved to be a sensible design decision when thrust balance and radial bearing issues were encountered during initial testing. Initial testing of the PTT turbopump is described by Rapp and Stapp [2]. Although useful for initial testing, the efficiency losses caused by the large shroud gap would not be a viable for the final turbine design. Likewise, the small gap required to meet the 90+% efficiency may not be reliable.

Completion of the final HP turbine design required further analysis of the blade shroud gap losses beyond a 1D solution. Experimental data describing shroud gap losses in radial inflow turbines operating with sCO2 is not currently available. However, correlations with other working fluids are plentiful. The work of Futral and Holeski [3] in 1970 is widely applied across numerous published radial inflow turbine designs, analyses, and experiments. The conclusions and data presented by Futral and Holeski [3] can be utilized to build a simple empirical model of total efficiency loss and mass flow rate change as a function of the blade tip clearance, inlet blade height, and outlet blade height. Futral and Holeski concluded radial shroud gap is dominant in efficiency loss and mass flow rate increase while axial tip clearance is a second order effect. Currently, their conclusions have been utilized in sCO2 turbine design work by Strang [4] and Qi [5] but has yet to be applied to an experiment or computational models exploring a range of shroud gaps or mass flow changes.

To characterize the shroud gap performance effects on the PTT Turbopump HP turbine and verify the 1D mean line design efficiency, eleven CFD models across a range of shroud gaps were constructed by the author and results were compared to simple linear equations from the conclusions made by Futral and Holeski [3].

COMPUTATIONAL MODELS

Eleven steady state (SS) Reynolds Averaged Naiver Stokes (RANS) CFD models with a shroud gaps between 0in (no gap ideal case) to 0.025in (0.635mm) were constructed in the ANSYS Workbench R19.2 environment using ANSYS Turbogrid and CFX. Turbine nozzle and blade geometry were obtained via AxSTREAM® output. A k-ω-SST turbulence model was employed along with second order discretization schemes [6]. The HPT rotor is comprised on 17 blades and nozzle is comprised of 8 vanes. Due to the unequal pitch between the rotor and stator a multiple frame of reference (MFR) mixing plane model was utilized at the interface between the rotating and static domains as described in Chapter 3 of [6].

ANSYS blade/design modeler was utilized to extract the geometry for meshing in Turbogrid. Sector domains with a single blade and vane were meshed for periodic symmetry. Resulting periodic angles were 45° for the stator and 21.176° for the rotor. All wall inflation layers except for the shroud gap were meshed based on a y+ = 1 with a Re = 1e6, and maximum inflation rate 1.5. These settings resulted in first cell heights in the range of 1e-6 in. Model results showed the Reynolds number setting should have been increased for the model to achieve y+ = 1 on all walls. However, this was not practical because first cell heights would likely enter the 1e-7 in range. First cell heights in this range would have resulted in cell length aspect ratios > 1000 or a cell count beyond available computation resources. A mesh that could achieve y+=1 and fully

resolve the viscous sublayer on all walls would have been preferable in these models. However, the automatic wall functionality in ANSYS CFX allows the solver to use wall functions in locations where the viscous sublayer cannot be fully resolved due to mesh limitations. This is detailed in work by Menter et al. [7]. Cell counts for the rotating domain ranged between 1,710,300 and 4,030,100. Maximum and minimum face angles were 161.5 and 25.8° respectively. The maximum edge length ratio was 798.9. A preferable edge length ratio would be less than 200 however this was not practical due to compute resources. Moreover, the larger aspect ratios cells are a consequence of the inflation layers required to capture wall effects and thus are oriented in the direction of flow. Inflation layers at the nozzle trailing edge are shown in Figure 2.

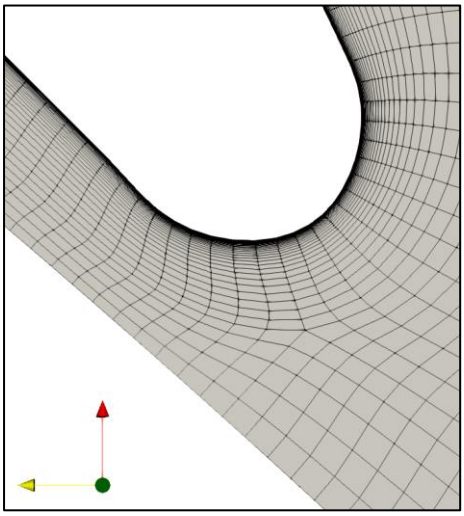

Figure 2: Inflation layers at the nozzle trailing edge

The uniform shroud gap for each model was generated using the shroud tip gap function in ANSYS blade modeler and was subsequently meshed in the corresponding feature in Turbogrid. This allowed tailoring of the shroud gap mesh as the normal distance between the blade tip and shroud wall increased. Number of elements across the gap varied between 50 and 100. The number of constant thickness elements across the gap was varied between 25 and 50 to achieve maximum expansion rates of ≈ 1.2.

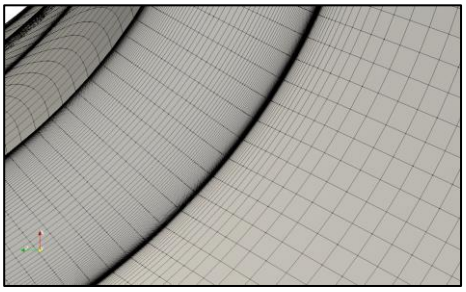

Figure 3: Shroud gap mesh between blade tip and wall

A single mesh was generated for the nozzle (stationary domain) and was utilized for all models. The stator mesh had a total of 860,750 cells. The maximum and minimum face angles were 131.8° and 41.9° respectively. The maximum edge length ratio was 876. Detailed mesh information for all domains is contained in Appendix A. Figures 4-6 provide overall views of rotor and stator mesh domains.

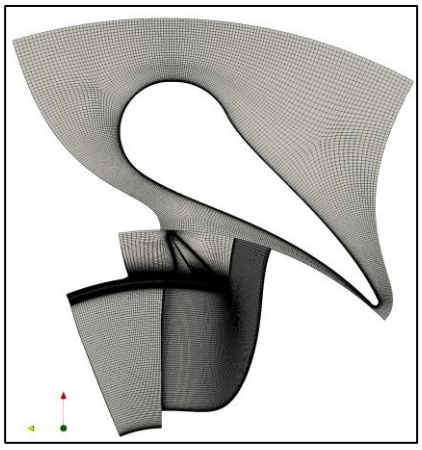

Figure 4: Rotor stator mesh with 0.025in shroud gap

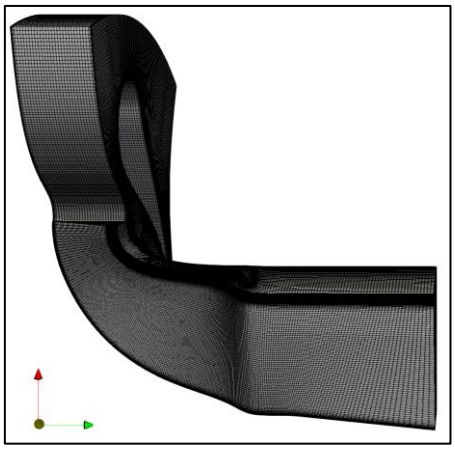

Figure 5: Rotor stator mesh with 0.025in shroud gap

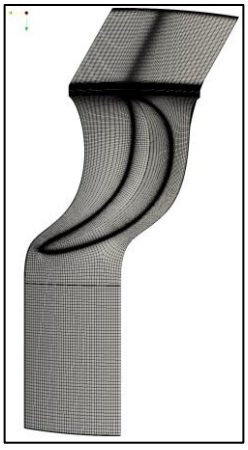

Figure 4: Rotor mesh with 0.025in shroud gap

Inflow and outflow boundary conditions were obtained from AxSTREAM® 1D results and were identical for all models. A total pressure (P_{t4} = 6135 psi (42.3 MPa)) and total temperature (T_{t4} = 1382.1 °F (1022.7 K)) boundary condition was applied at the inlet. An average static pressure (P_{s5} = 4322 psi (29.8 MPa)) boundary condition was applied at the outlet. A constant 118,350 rpm angular velocity was imposed on the rotating domain for all models. Additionally, the shroud wall in rotating domain was counter rotated to appropriately simulate the shearing between the blade tips and shroud wall. These constant boundary conditions are consistent with the experimental parameters and results presented by Futral and Holeski [3]. Periodic rotational symmetry boundary conditions were imposed on the rotating and static domains according to their respective pitch angles. Lastly, an MFR mixing plane interface was applied between the rotating and static domain [6].

A real gas CO2 model was applied to all model via ANSYS .rgp files/tables generated from NIST REFPROP [8]. The table utilized encompassed temperatures between 89.3 °F (305 K) - 2000°F (1366 K) and pressure between 1058.775 psi (7.3 MPa) - 6961.811 psi (48 MPa). The large temperature and pressure range of the table was selected to ensure solver stability.

All models utilized high resolution (2nd order) discretization for turbulence numerics and the advection scheme. Additionally, A physical timescale of 1e-6 seconds was employed across all solvers. Total – total isentropic efficiency, outlet total pressure (P_{t5}), and power output values were monitored for all solutions to aid in judging model convergence. RMS residual targets for all conserved variables was set to 1e-5 and the conservation target was set to 0.01. Figure 7 details final RMS residuals achieved for each model. The residual target of 1e-5 could not be achieved for all variables across all models. Inspection of the monitored values showed steady behavior thus the models were determined sufficiently converged for their intended purpose of evaluating changes in isentropic efficiency and mass flow rate.

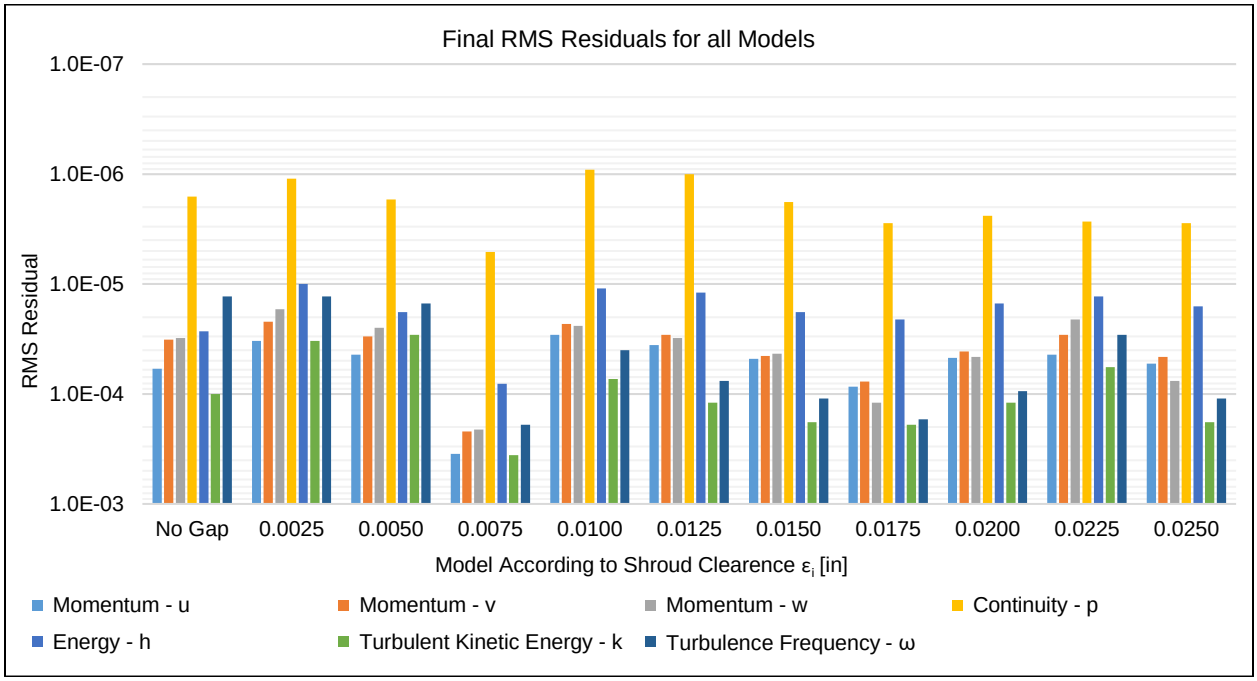

Figure 5: Final RMS residuals for all models

RESULTS AND DISCUSSION

The conclusions presented by Futral and Holeski [3] for total efficiency loss and mass flow rate increase are defined in terms of shroud gap as a percentage of blade height. This quantity is represented in this work by $\varepsilon\%b$ and defined by Equation 1. From their experimental data, Futral and Holeski concluded the following decreases in efficiency and changes in mass flow rate. First, a 1% increase in axial clearance as a percentage of inlet blade height ($\varepsilon_x\%b_{4.1}$) resulted in 0.15% decrease in total efficiency and a 0.1% increase in mass flow rate. Second, a 1% increase in radial clearance as a percentage of outlet blade height ($\varepsilon_r\%b_{4.3}$) resulted in 1.6% decrease in total efficiency and a 0.3% increase in mass flow rate. These conclusions by Futral and Holeski are formed into the linear equations defined in Equations 2 and 3.

Equation 1: $$\varepsilon\%b = \frac{\varepsilon}{b}$$

Equation 2: $$\Delta\eta_{tt} = \left(\frac{-0.0015\varepsilon_x}{b_{4.1}} - \frac{0.016\varepsilon_r}{b_{4.3}}\right) = -\varepsilon_i\left(\frac{0.0015}{b_{4.1}} + \frac{0.016}{b_{4.3}}\right) \quad when\ \ \varepsilon_i = \varepsilon_r = \varepsilon_x$$

Equation 3: $$\Delta W = \left(\frac{-0.001\varepsilon_x}{b_{4.1}} + \frac{0.003\varepsilon_r}{b_{4.3}}\right) = \varepsilon_i\left(\frac{-0.001}{b_{4.1}} + \frac{0.003}{b_{4.3}}\right) \ \ when\ \ \varepsilon_i = \varepsilon_r = \varepsilon_x$$

Futral and Holeski defined their conclusions as valid for an axial clearance range of 1%-7% and a radial clearance range of only 1%-3% because the efficiency decrement beyond 3% reduces to less than 1.6% per 1% of blade height. This fact is taken into account in comparing the results of the computational models to the losses predicted by Equation 2. Results presented below also extrapolate Equations 2 and 3 to because the computational models in this work cover axial clearances up to 12.4% of inlet blade height. Passage dimensions for the PTT Turbopump a contained in Table 2.

Table 2: PTT Turbopump HPT Passage Dimensions

Inlet Passage Height ($b_{4.1}$) [in] =	0.20
Outlet Passage Height ($b_{4.3}$) [in] =	0.35

The CFX CFD model predicted a 91.6% total – total isentropic efficiency and a mass flow rate of 12.22 lbm/s (5.54 kg/s) for the no gap (ideal case). The case with a 0.005 in (0.127 mm) shroud gap resulted in a total – total isentropic efficiency 1.7% less than the 90.4% predicted by AxSTREAM®.

Passage dimensions defined in Table 2 and shroud gaps dimensions for each CFD model were applied to Equations 2 and 3 to produce predicted efficiency decrements and mass flow rate changes. Likewise, efficiency and mass flow rate results from each CFD model with a shroud gap were subtracted from the no shroud gap (ideal) model results to calculate efficiency decrements and mass flow rate changes. Results are detailed in Figures 8 and 9.

The efficiency results of the CFD models for gaps between 0.0025 in – 0.015 in ($1.2\% \leq \varepsilon_x\%b_{4.1} \leq 7.5\%$) and ($0.7\% \leq \varepsilon_r\%b_{4.3} \leq 4.2\%$) agree well with the efficiency decreases predicted Equation 2. Beyond a shroud of 0.015 in Equation 2 begins to over predict the efficiency loss. This over prediction is commensurate with previously mentioned conclusions made by Futral and Holeski [3].

The mass flow rate results of the CFD models do not agree well with the mass flow rate changes predicted by Equation 3. With a shroud gap of 0.0025in ($\varepsilon_x\%b_{4.1} = 1.2\%$) and ($\varepsilon_r\%b_{4.3} = 0.7\%$), Equation 3 underpredicts the mass flow rate increase by over 7.5x. However, the underprediction decreases to 1.5x with a shroud gap of 0.025in ($\varepsilon_x\%b_{4.1} = 12.4\%$) and ($\varepsilon_r\%b_{4.3} = 7\ \%$). Further, investigation of the CFD model results, including qualitative interrogation of flow field will likely be required to better understand the disagreement between the two models. The author suspects the disagreement is related to high density and low viscosity of sCO2.

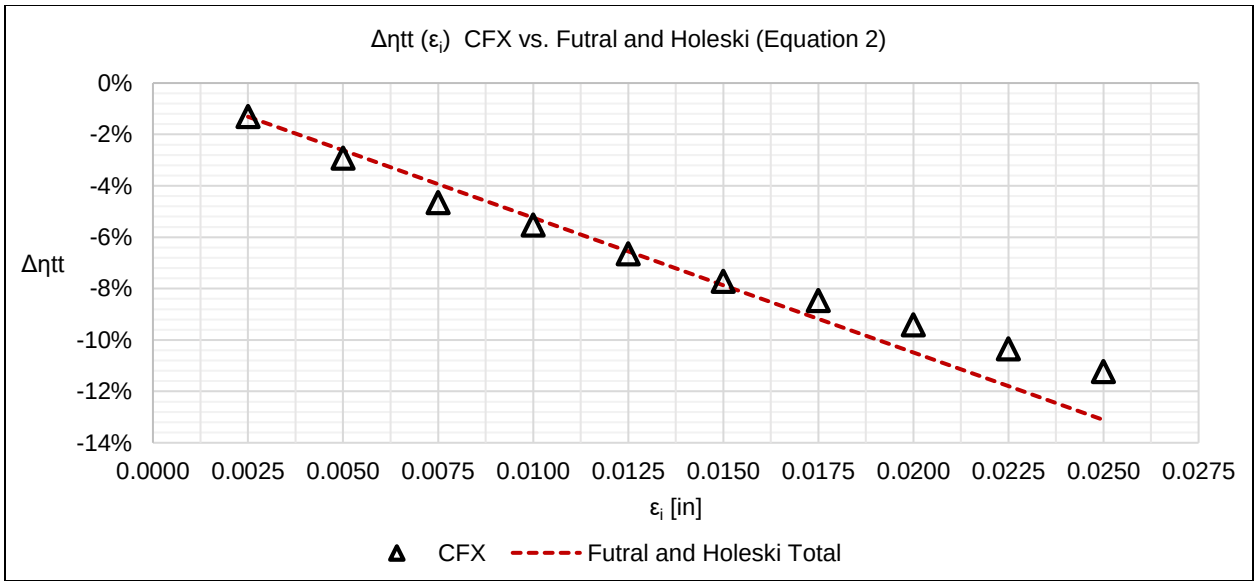

Figure 6: Change in total efficiency predicted by CFX model vs. Futral and Holeski correlation

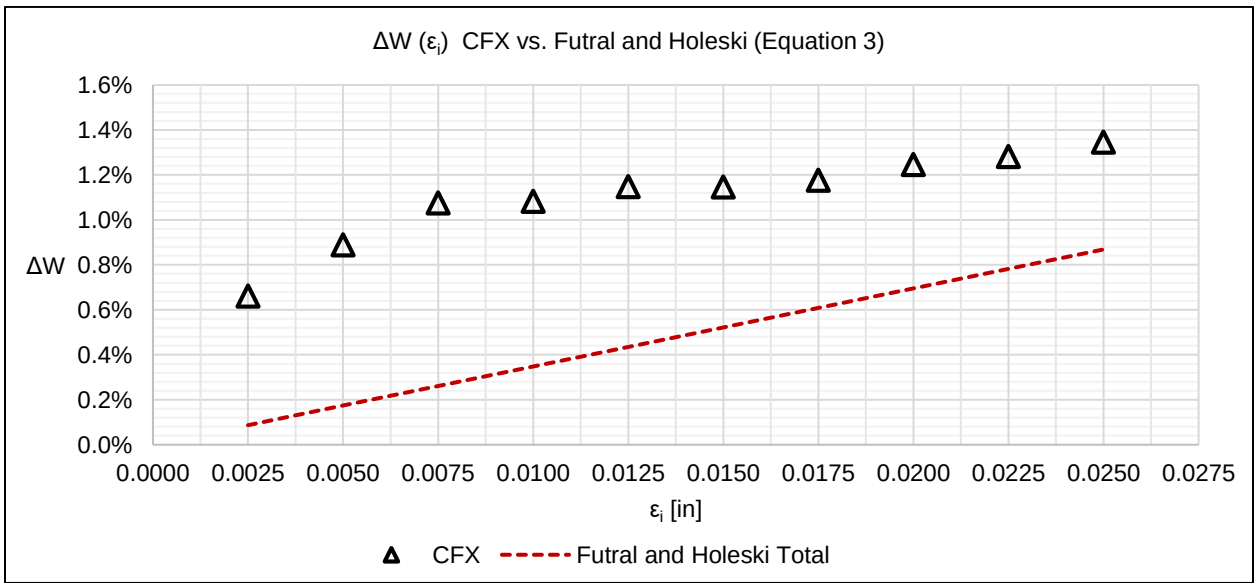

Figure 7: Change in mass flow rate predicted by CFX model vs. Futral and Holeski correlation

CONCLUSION

3D computational fluid dynamics (CFD) models with varying blade tip shroud clearances were constructed in ANSYS CFX to evaluate efficiency losses and mass flow rate changes of the Peregrine Turbine Technologies 1MW HP Turbine. CFD model results were compared to existing models used for determining shroud gap losses in non-supercritical turbomachinery. Results revealed agreement between existing efficiency decrement models by Futral and Holeski [3] across low ranges of shroud gaps as a percent of blade height. Digitization of the Futral and Holeski data plots and polynomial curve fitting would likely result in agreement between the models for larger shroud gaps. This approach appears to have been performed by Qi et al. [5] for design purposes. CFD model mass flow rates did not agree well with compared model. Further investigation of the CFD model results is required.

REFERENCES

[1] D. Fleming and A. Kruizenga, "Identified Corrosion and Erosion Mechanisms in SCO2 Brayton Cycles," Sandia National Laboratories, 2014.

[2] L. Rapp and D. Stapp, "Experimental Testing of a 1MW sCO2 Turbocompressor," in *3rd European supercritical CO2 Conference*, Paris, France, 2019.

[3] S. M. Futral and D. E. Holeski, "Experimental results of varying the blade-shroud clearance in a 6.02 inch radial inflow turbine," National Aeronautics and Space Administration, Washington, D.C., 1970.

[4] T. Strang, "Aerodynamic Design of a Supercritical Carbon Dioxide Radial Inflow Turbine using Meanline and Computational Methods," Carleton University Department of Mechanical and Aerospace Engineering, Ottawa, Ontario, 2018.

[5] J. Qi, T. Reddell, K. Qin, K. Hooman and I. H. J. Jahn, "Supercritical CO2 Radial Turbine Design Performance as a Function of Turbine," *ASME Journal of Turbomachinery,* 2017.

[6] ANSYS, Inc, ANSYS CFX-Solver Theory Guide 2019R3, 2019.

[7] F. Menter, J. Carregal Ferreira, T. Esch and B. Konno, "The SST Turbulence Model with Improved Wall Treatment for Heat Transfer Predictions in Gas Turbines," in *Proceedings of the International Gas Turbine Congress 2003 Tokyo*, Tokyo, 2003.

[8] National Institute of Standards and Techology, "NIST REFPROP," [Online]. Available: https://www.nist.gov/srd/refprop.

APPENDIX A. MESH SETTINGS AND METRICS

Shroud Gap [in]	0.0000	0.0025	0.0050	0.0075	0.0100	0.0125	0.0150	0.0175	0.0200	0.0225	0.0250	Stator
Mesh Size												
Method	Global Size Factor	←	←	←	←	←	←	←	←	←	←	←
Size Factor	1.25	1	1	1	1	1	1	1	1	1	1	1
Boundary Layer Refinement Control, Method	First Element Offset	←	←	←	←	←	←	←	←	←	←	←
Offset y+	1	1	1	1	1	1	1	1	1	1	1	1
Target Maximum Expansion Rate	X	X	X	X	X	X	X	X	X	X	X	X
Rate	1.5	1.5	1.5	1.5	1.2	1.5	1.3	1.5	1.5	1.5	1.5	1.5
Near wall element size specification, Method	y+	y+	y+	y+	y+	y+	y+	y+	y+	y+	y+	y+
Reynolds No.	1.00E+06	1.00E+06	1.00E+06	1.00E+06	1.00E+06	1.00E+06	1.00E+06	1.00E+06	1.00E+06	1.00E+06	1.00E+06	1.00E+06
Five Edge Vertex Mesh Size Reduction, Factor	0.5	0.75	0.75	0.75	0.75	0.75	0.75	0.75	0.75	0.75	0.75	0.5
Inlet Domian												
Outlet Domain	X	X	X	X	X	X	X	X	X	X	X	
Passage												
Spanwise Blade Distribution Parameters												
Method	Element Count and Size	←	←	←	←	←	←	←	←	←	←	←
# of Elements	100	100	100	100	100	100	100	100	100	100	100	50
Const Elements	50	50	50	50	50	50	50	50	50	50	50	25
Size of Elements Nex to Wall (y+), Hub	1	1	1	1	1	1	1	1	1	1	1	1
Size of Elements Nex to Wall (y+), Shroud	1	N/A	N/A	N/A	N/A	N/A	N/A	N/A	N/A	N/A	N/A	1
Expansion Rate	1.23746	1.23703	1.23659	1.23615	1.2357	1.23525	1.2348	1.23434	1.23389	1.23342	1.23296	1.59749
Boundary Layer												
Near Wall Expansion Rates, Minimum	1.24436	1.22997	1.22997	1.22997	1.05548	1.22997	1.09863	1.22993	1.22993	1.22993	1.22993	1.15239
Near Wall Expansion Rates, Maximum	1.53722	1.55117	1.55117	1.55115	1.25464	1.55114	1.32731	1.55071	1.5507	1.5507	1.55069	1.53277
Outlet												
Outlet Domain												
Mesh Type	H-Grid	H-Grid	H-Grid	H-Grid	H-Grid	H-Grid	H-Grid	H-Grid	H-Grid	H-Grid	H-Grid	N/A
Define By	Target Number of	←	←	←	←	←	←	←	←	←	←	N/A
# of Elements	50	50	50	50	50	50	50	50	50	50	50	N/A
Shroud Tip												
Shroud Tip Distribution Parameters												
Method	N/A	Element Count and Size										N/A
# of Elements	N/A	50	50	75	75	75	100	100	100	100	100	N/A
Const Elements	N/A	25	25	30	35	35	50	50	50	50	50	N/A
Expansion Rate	N/A	1.05683	1.10431	1.06767	1.07968	1.0888	1.06243	1.06701	1.07094	1.07437	1.07742	N/A
Size of Elements Next to Wall (y+)												
Tip	N/A	1	1	1	1	1	1	1	1	1	1	N/A
Shroud	N/A	1	1	1	1	1	1	1	1	1	1	N/A
Blade Tip												
Overide Target Max Expansion Rate	N/A	X	X	X	X	X	X	X	X	X	X	N/A
Rate	N/A	1.2	1.2	1.2	1.2	1.2	1.2	1.2	1.2	1.2	1.2	N/A
Near Wall Expansion Rates, Minimum	N/A	1.0129	1.0135	1.01921	1.02093	1.02147	1.02132	1.02065	1.005567	1.03119	1.03168	N/A
Near Wall Expansion Rates, Maximum	N/A	1.20835	1.20816	1.20797	1.20779	1.20762	1.20745	1.20729	1.20713	1.20706	1.20691	N/A
Mesh Statistics												
Minimum Face Angle [°]	31.0491	25.838	26.3496	26.055	26.3659	29.5244	31.1747	31.6638	31.8193	32.0203	32.5392	41.9514
Maximum Face Angle [°]	148.956	160.546	160.598	161.351	161.455	161.459	161.384	161.454	160.305	161.399	161.413	131.777
Maximum Element Volume Ratio	2.76566	3.94996	4.14187	3.8336	3.89916	3.95803	4.17024	4.18388	4.13853	4.10317	4.05429	3.47857
Minimum Volume [m^3]	2.47E-18	3.09E-18	3.07E-18	3.06E-18	2.92E-18	3.04E-18	3.02E-18	3.01E-18	3.00E-18	2.98E-18	2.97E-18	8.48E-18
Maximum Edge Length Ratio	613.133	770.561	772.296	774.993	777.881	785.009	787.101	789.82	793.449	795.819	798.921	875.941
Maximum Connectivity Number	10	10	10	10	10	10	10	10	10	10	10	10
Total Cells	1710300	2488100	2488100	3134550	3528300	3134550	4030100	3750300	3750300	3768100	3768100	860750

Dependent	Input